Improvements to MASS turbulence profile estimation at Paranal

Timothy Butterley[a], Marc Sarazin[b], Julio Navarrete[b], James Osborn[a], Ollie Farley[a], and Miska Le Louarn[b]

[a]Centre for Advanced Instrumentation, Department of Physics, University of Durham, South Road, Durham, DH1 3LE, UK

[b]European Southern Observatory (ESO), Karl-Schwarzschild-Str. 2, D-85748 Garching, Germany

ABSTRACT

The multi-aperture scintillation sensor (MASS) is a widely-used robotic turbulence profiling instrument that measures the turbulence strength in 6 altitude resolution elements centred at 0.5, 1, 2, 4, 8 and 16 km. Paranal Observatory has a facility MASS instrument that is used to support adaptive optics operations. The observatory also has a stereo scintillation detection and ranging (S-SCIDAR) instrument that is typically operated for several nights per month, measuring the full turbulence profile with a resolution of several hundred metres.

We make a comparison between concurrent S-SCIDAR and MASS measurements by binning the S-SCIDAR profiles according to the MASS response functions and performing a layer-by-layer comparison of the 6 MASS layers. We show that some layers tend to be significantly over- or underestimated by MASS, compared to S-SCIDAR, but the sum of all 6 layers is quite consistent between the two instruments.

We present a detailed Monte Carlo simulation of the MASS instrument, using S-SCIDAR profiles as inputs to reproduce realistic MASS output raw data. By comparing simulated raw data with real measurements we verify the physical operation of the MASS instrument and validate the simulation code as a tool to investigate the profile restoration problem.

Keywords: MASS, SCIDAR, turbulence profiling, Paranal

1. INTRODUCTION

Paranal observatory operates a number of turbulence profiling instruments including a multi-aperture scintillation sensor (MASS)[1,2] and a stereo scintillation detection and ranging (S-SCIDAR)[3] instrument. MASS is a robotic instrument that measures the free atmosphere turbulence profile with coarse resolution every night. S-SCIDAR measures the complete profile with high resolution several nights per month. MASS and S-SCIDAR do not agree on the C_n^2 profile; comparisons with other instruments on the site suggest MASS is responsible. The aim of this study is to investigate the discrepancy and find a solution.

2. MASS VS S-SCIDAR COMPARISON

This section contains a brief comparison of simultaneous MASS and S-SCIDAR data in order to quantify the discrepancy between the instruments.

The vertical resolution of S-SCIDAR is much higher than that of MASS. The S-SCIDAR profiles can be binned into 6 resolution elements according to the (idealised) MASS response functions (shown in figure 1), yielding "synthetic" MASS profiles that one would expect to be identical (statistical errors aside) if the two instruments were observing in the same direction. In practice they will generally be observing different targets but this should translate to more scatter rather than systematic differences between the two sets of profiles.

Further author information: (Send correspondence to T.B.)
T.B.: E-mail: timothy.butterley@durham.ac.uk, Telephone: +44 191 334 3714

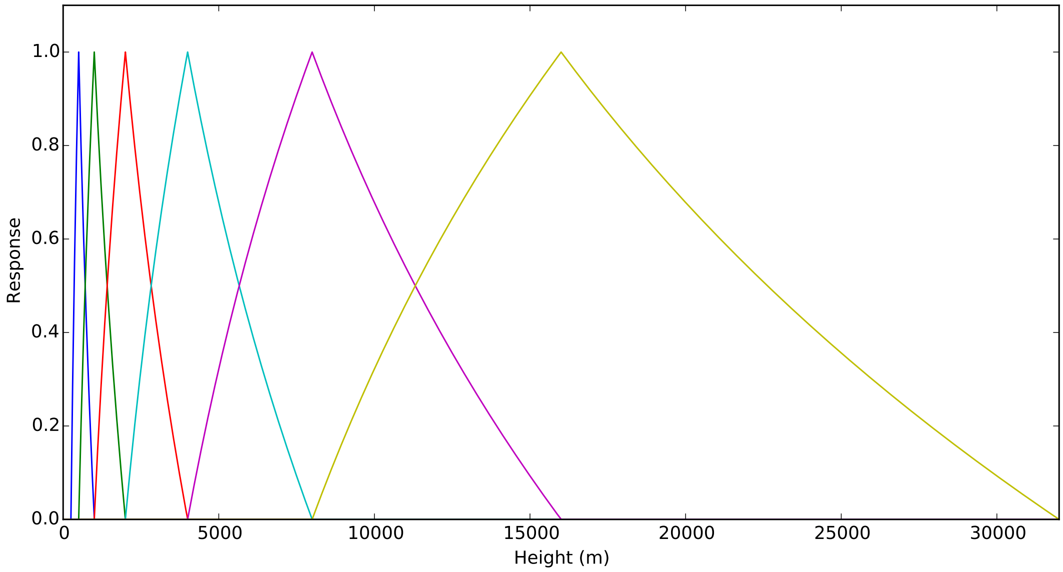

Figure 1. MASS response functions. These show how turbulence at a given height contributes to signal in the MASS layers. Note that these functions would be triangular if the x-scale was logarithmic.

Previous comparisons between MASS and SCIDAR measurements made at Paranal have been carried out by Masciadri *et al* and Lombardi *et al*.[4,5] These comparisons used data from a different SCIDAR instrument (a conventional generalized SCIDAR) and the MASS data were processed using different software so we do not necessarily expect to obtain results that are in agreement with these earlier studies.

We follow the Lombardi approach here. Lombardi compared the instruments in terms of $\log(J)$ where J is C_n^2 integrated over an altitude range. The main parameter is

$$k = 10^c \tag{1}$$

where

$$c = \frac{1}{N}\sum_{n=1}^{N}\left[\log(J_{MASS,n}) - \log(J_{S-SCIDAR,n})\right]. \tag{2}$$

It follows that

$$J_{MASS} = kJ_{S-SCIDAR}. \tag{3}$$

Figure 2 shows a scatter plot for the sum of all 6 MASS layers. Figure 3 shows separate scatter plots for each of the 6 layers. The values of k, c and the Pearson correlation coefficient are shown on each plot.

MASS is shown to overestimate the strength of layer 1 (at 500 m) and underestimate layers 3 and 5 (at 2 km and 8 km respectively) compared to S-SCIDAR. The scatter is greatest in layer 1, which makes sense given that scintillation from this layer is weakest. The estimate of the total of all 6 layers is more robust.

The fit coefficients are shown in table 1. This includes estimated uncertainties that were produced via the bootstrapping method, which works as follows: the dataset was resampled randomly, with replacement, producing a sample the same size as the original. The various metrics were recalculated from the resampled data. This process was repeated many times, producing a distribution of values for each metric. The uncertainties shown represent 95 % confidence intervals measured from these distributions.

Layer	$\log(J)$ linearity coefficient k
1	2.2 ± 0.1
2	0.87 ± 0.03
3	0.41 ± 0.02
4	1.06 ± 0.03
5	0.28 ± 0.01
6	1.13 ± 0.02
FA	0.91 ± 0.01

Table 1. Fit coefficients for MASS vs S-SCIDAR. Uncertainties shown are 95 % confidence intervals that were estimated using the bootstrap method.

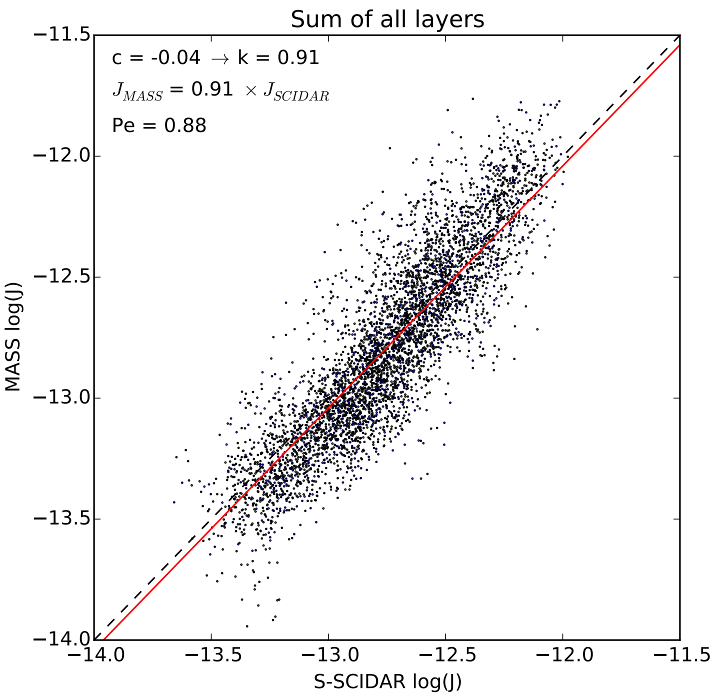

Figure 2. Comparison of log of total integrated $C_n^2(h)$ from the 6 MASS layers from S-SCIDAR vs MASS. The broken line shows $y = x$ i.e. the case where the two instruments agree perfectly and the red line shows a linear fit through the origin.

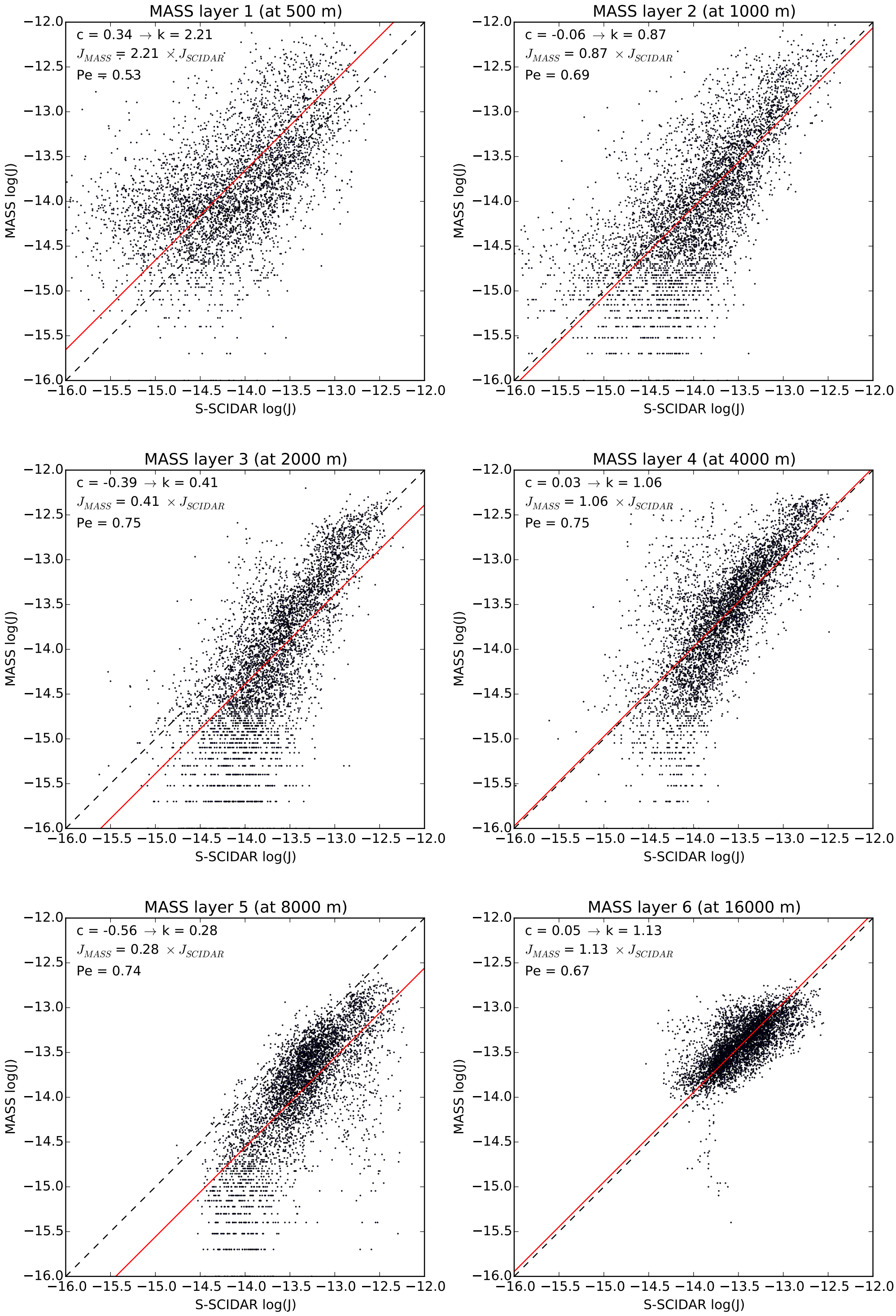

Figure 3. Comparison of log of integrated $C_n^2(h)$ due to each of the 6 MASS layers from S-SCIDAR vs MASS. On each plot the broken lines shows $y = x$ i.e. the case where the two instruments agree perfectly and the red line shows a linear fit through the origin.

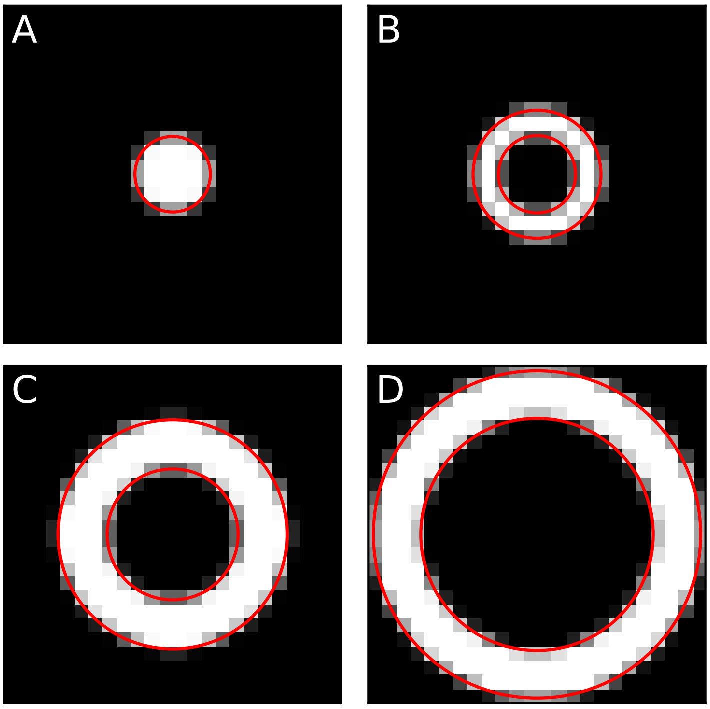

Figure 4. MASS aperture functions. Although shown separately here, the 4 apertures are arranged concentrically in the pupil plane of the instrument.

3. MASS SIMULATION TOOL

To assist in investigating the discrepancies between MASS and S-SCIDAR, an end-to-end Monte Carlo simulation of the MASS instrument has been developed. The following physical effects are modelled:

- **Atmospheric propagation** – a physical optical propagation model of light through the turbulent atmosphere is required to produce the scintillation signal seen by MASS.
- **Chromatic effects** – this includes variation in scintillation with wavelength, the colour of the target star and the response curve of the detectors and optics.
- **Temporal effects** – finite exposure times/dataset duration and different wind speeds.
- **Photon/detector noise** – MASS uses photomultiplier tubes, which have different noise characteristics to CCDs.

The simulation code consists of a series of distinct components. This section describes each component in turn.

3.1 Atmosphere model

The atmosphere is modelled as a series of Von Karman phase screens. Fresnel propagation is used to obtain the intensity field at the ground. The MASS pupil, consisting of 4 concentric apertures as shown in figure 4, is translated across the intensity field to simulate the wind. The integrated flux in each aperture is evaluated at each step. Propagation is monochromatic; it is repeated at 6 different wavelengths (360, 414, 468, 522, 576, 630 nm).

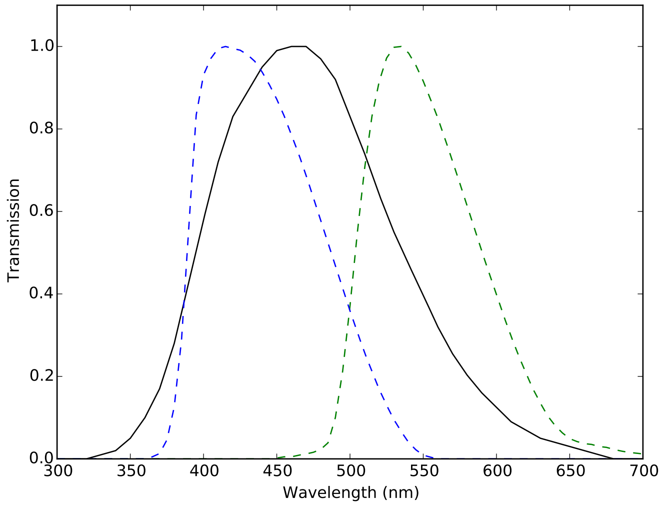

Figure 5. Instrument response (black line) including all optical surfaces, the atmosphere and the detector. The blue and green broken lines show the Johnson B and V filters respectively.

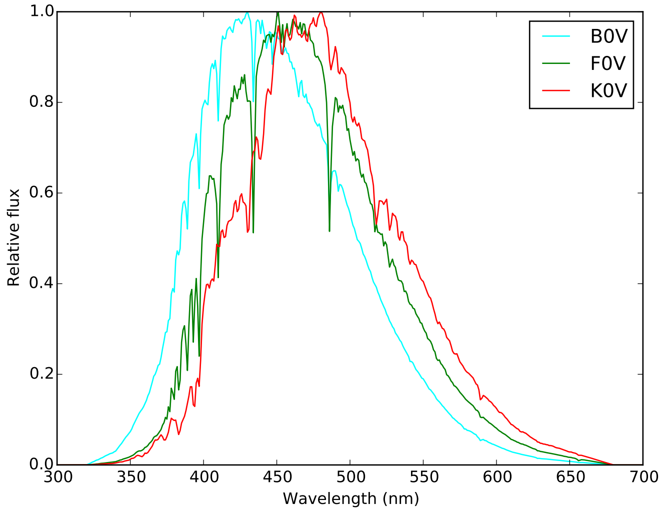

Figure 6. Relative flux detected by MASS for different stellar spectral types.

3.2 Chromatic effects

MASS does not have a filter; its photometric band is determined by the optics and detector (see figure 5). For each target, a model stellar spectrum is taken from the UVILIB library[6] and scaled by the instrument response curve. The result (figure 6) determines the weights for combining the monochromatic fluxes from the atmospheric simulation.

3.3 Temporal effects

We assume all atmospheric layers translate at the effective wind velocity, which is calculated from S-SCIDAR profiles. In high wind speeds the intensity "smears", reducing the scintillation index as shown in figure 7.

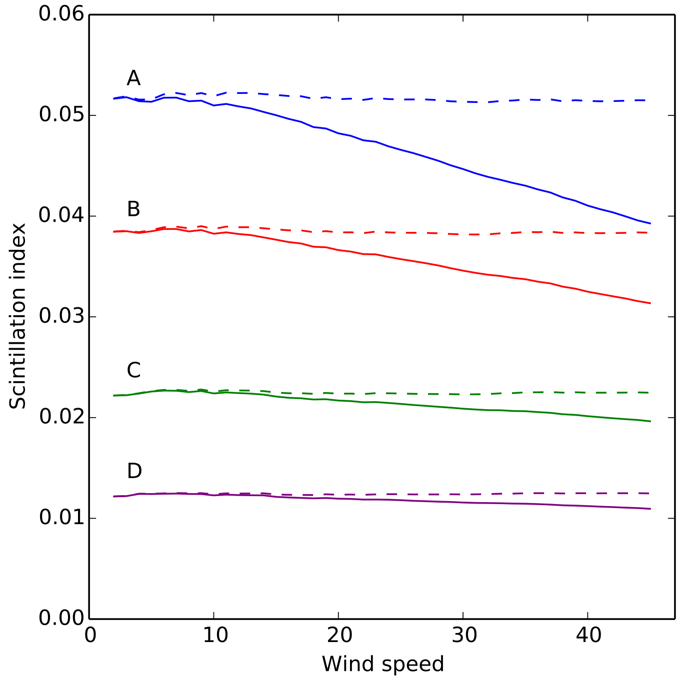

Figure 7. Example of scintillation index in each MASS aperture as a function of wind speed for a realistic turbulence profile. The broken lines represent the instantaneous case where the scintillation pattern is "frozen" in each exposure.

3.4 Detectors

The detectors are photon-counting photomultiplier tubes (PMTs). The PMTs have a 15 ns dead time, which has the effect of attenuating the signal at high flux. We model the arrival times of individual photons – the interarrival time has an exponential distribution. We discard any photons that arrive within the dead time after a photon is detected.

3.5 Data reduction

The output of the simulation corresponds to reduced data (prior to profile restoration) from MASS. Reduced MASS data simply takes the form of the flux variance in each of the 4 concentric apertures and covariances between fluxes in different apertures.

4. SIMULATION RESULTS

We have ∼5000 pairs of simultaneous MASS and S-SCIDAR measurements. For a given S-SCIDAR profile, corrected for MASS airmass, we can simulate the expected flux variances seen by the MASS. Figure 8 shows a comparison between real and measured flux variances and covariances for a sample of 268 MASS/S-SCIDAR measurements.

The simulated measurements are in good agreement with real measurements, except for the regime where the scintillation is particularly strong. The scatter is down to the different pointing directions of MASS and S-SCIDAR. These results validate the simulation as a suitable tool for investigating the MASS profile restoration problem.

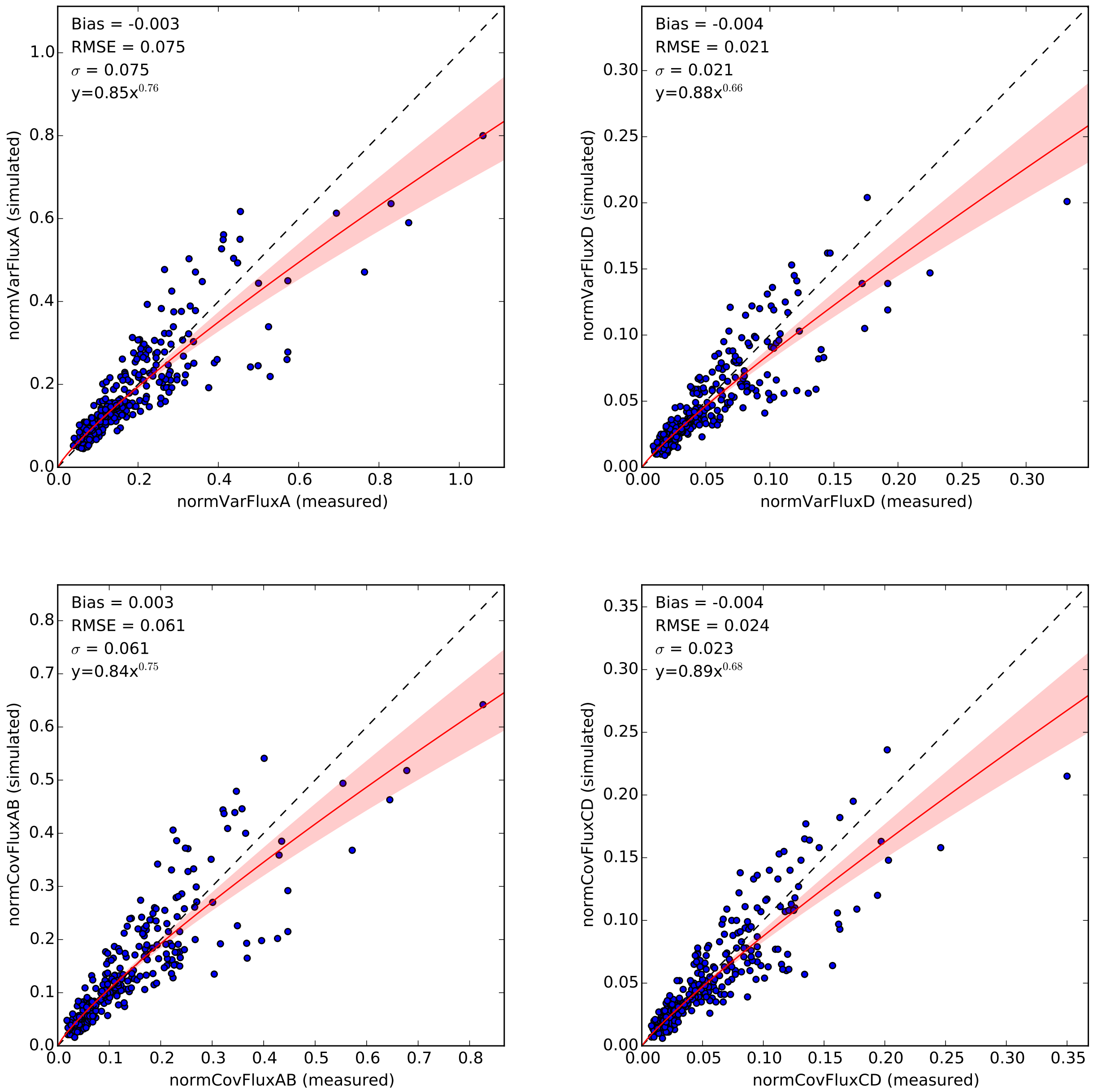

Figure 8. MASS aperture flux variances and covariances, simulated using S-SCIDAR profiles, plotted against real MASS measurements. Upper left: aperture A variance; upper right: aperture D variance; lower left: covariance between apertures A and B; lower right: covariance between apertures C and D.

5. CONCLUSIONS

MASS and S-SCIDAR at Paranal yield inconsistent turbulence profiles. An end-to-end Monte Carlo model of the MASS instrument has been developed as a tool for investigating the discrepancy. The model has been verified by reproducing simulated data comparable to real data from MASS, albeit with some systematic errors in strong scintillation. The model will be used to investigate the MASS profile restoration problem.

ACKNOWLEDGMENTS

This study has been funded by the European Southern Observatory (ESO). TB and JO are grateful to the Science and Technology Facilities Committee (STFC) for financial support (grant reference ST/P000541/1). OF is also grateful to STFC for financial support (grant reference ST/N50404X/1).

REFERENCES

[1] Tokovinin, A., Kornilov, V., Shatsky, N., and Voziakova, O., "Restoration of turbulence profile from scintillation indices," MNRAS **343**, 891–899 (2003).

[2] Kornilov, V., Tokovinin, A., Shatsky, N., Voziakova, O., Potanin, S., and Safonov, B., "Combined MASS-DIMM instruments for atmospheric turbulence studies," MNRAS **382**, 1268–1278 (2007).

[3] Osborn, J., Wilson, R. W., Sarazin, M., Butterley, T., Chacón, A., Derie, F., Farley, O. J. D., Haubois, X., Laidlaw, D., Le Louarn, M., Masciadri, E., Milli, J., Navarrete, J., and Townson, M. J., "Optical turbulence profiling with Stereo-SCIDAR for VLT and ELT," MNRAS **478**, 825–834 (2018).

[4] Masciadri, E., Lombardi, G., and Lascaux, F., "On the comparison between MASS and generalized-SCIDAR techniques," MNRAS **438**, 983–1004 (2014).

[5] Lombardi, G. and Sarazin, M., "Using MASS for AO simulations: a note on the comparison between MASS and Generalized SCIDAR techniques," MNRAS **455**, 2377–2386 (2016).

[6] Pickles, A. J., "A Stellar Spectral Flux Library: 1150-25000 Å," PASP **110**, 863–878 (1998).